# Ultrafast Terahertz Probes of Charge Transfer and Recombination Pathway of $CH_3NH_3PbI_3$ Perovskites *

Hui-Jie Yan(严慧婕)[1], Zhi-Liang Ku(库治良)[2], Xue-Feng Hu(胡雪峰)[1], Wan-Ying Zhao(赵婉莹)[1], Min-Jian Zhong(钟敏建)[1], Qi-Biao Zhu(朱绮彪)[1], Xian Lin(林贤)[1], Zuan-Ming Jin(金钻明)[1**], Guo-Hong Ma(马国宏)[1**]

[1]*Department of Physics, Shanghai University, Shanghai 200444*
[2]*State Key Laboratory of Advanced Technology For Materials Synthesis and Processing, Wuhan University of Technology, Wuhan 430070*

(Received 21 September 2017)

*We use transient terahertz photoconductivity measurements to demonstrate that upon optical excitation of $CH_3NH_3PbI_3$ perovskite, the hole transfer from $CH_3NH_3PbI_3$ into the organic hole-transporting material (HTM) Spiro-OMeTAD occurs on a sub-picosecond timescale. Second-order recombination is the dominant decay pathway at higher photo-excitation fluences as observed in neat $CH_3NH_3PbI_3$ films. In contrast, under similar experimental conditions, second-order recombination weakly contributes the relatively slow recombination between the electrons in the perovskite and the injected holes in HTM, as a loss mechanism at the $CH_3NH_3PbI_3$/Spiro-OMeTAD interface. Our results offer insights into the intrinsic photophysics of $CH_3NH_3PbI_3$-based perovskites with direct implications for photovoltaic devices and optoelectronic applications.*

*PACS:* 84.60.Jt, 78.47.−p, 07.57.Ty DOI: 10.1088/0256-307X/35/2/028401

Organic–inorganic hybrid systems based on lead halide compound have recently achieved considerable success as light harvesters in solid-state solar cells.[1−6] Several groups have reported power conversion efficiencies (PCEs) from 10% to 20% for solution processed organometal halide perovskite (OMHP)-based solar cells in the past five years. Slow electron–hole recombination and persistent high mobility are essential features for an efficient solar cell.[7−10] The fundamental photophysical processes underlying solar cell function need to be understood to fully utilize the properties of these materials. Further work is needed to obtain clearer correlations among spectroscopic absorbance, transport, sample structure, interface, defect, excitation condition, and so on.[11,12]

The charge transport in ordered crystalline semiconductors is largely delocalized. The photocarrier lifetime is defined by the mechanisms of photocarrier energy dissipation.[13−15] In contrast, the recovery kinetics in perovskites is modelled by the rate equation,[16] $-\frac{dn(t)}{dt} = k_1 n + k_2 n^2 + k_3 n^3$, where $n$ is the photogenerated carrier density, and $k_1$–$k_3$ represent the monomolecular process (trap-assisted recombination), bimolecular process (free carrier recombination) and trimolecular process (nonradiative Auger recombination), respectively. Indeed, to elucidate the role of free carriers and the carrier transfer between OMHP and electron- or hole-acceptor materials would provide a deeper understanding of the mechanisms that give rise to the high performance of hybrid perovskite-based solar cell devices.[17]

Generally, by using various time-resolved spectroscopic techniques, such as transient absorption and photoluminescence spectroscopy, the quenching of the photo-induced absorption or suppression of the fluorescence of OMHP in the presence of Spiro-OMeTAD (extensively used as a hole transport material (HTM)) has been observed qualitatively to investigate the hole injection dynamics.[18−23] In this work, we applied time-resolved terahertz spectroscopy to focus on the carrier dynamics of all occurring photo-induced charge transfer processes and to derive the effective mechanism for charge separation at the $CH_3NH_3PbI_3$/Spiro-OMeTAD interface. Our quantitative information is important for understanding the mechanism of the devices and eventually for the improvement of their photovoltaic performances.

To prepare the $CH_3NH_3PbI_3$ film, the $PbI_2$ film was firstly deposited on the quartz slide by spin-coating a $PbI_2$ solution (462 mgml$^{-1}$ in DMF) at 3000 rpm for 30 s. After drying at 70℃, the as-prepared $PbI_2$ film was dipped in a solution of $CH_3NH_3I$ in 2-propanal (10 mgml$^{-1}$ for 20 s and rinsed with 2-propanal, followed by annealing at 100℃ for 1 min in a glove-box. For the $CH_3NH_3PbI_3$/Spiro-OMeTAD film,

*Supported by the National Natural Science Foundation of China under Grant Nos 11674213, 11604202 and 61735010, the Young Eastern Scholar at Shanghai Institutions of Higher Learning under Grant No QD2015020, the Universities Young Teachers Training Funding Program under Grant No ZZSD15098, and the 'Chen Guang' Project of Shanghai Municipal Education Commission and Shanghai Education Development Foundation under Grant No 16CG45.

**Corresponding author. Email: physics_jzm@shu.edu.cn; ghma@staff.shu.edu.cn

© 2018 Chinese Physical Society and IOP Publishing Ltd

the Spiro-OMeTAD was deposited on top of the as-prepared $CH_3NH_3PbI_3$ film by spin-coating a Spiro-MeOTAD solution containing 0.17 M Spiro-MeOTAD, 0.198 M 4-tert-butylpyridine (TBP) and 0.064 M lithium bis(trifluoromethylsul-phonyl)imide (LiTFSI) in chlorobenzene at 3000 rpm for 30 s. In our measurements, the films of $CH_3NH_3PbI_3$ and $CH_3NH_3PbI_3$/Spiro-OMeTAD were deposited on fused silica substrates. Our deposited films had an average thickness of 400 nm±100 nm. The samples were characterized by UV-visible absorption spectrum, scanning electron microscopy (SEM) and x-ray diffraction (XRD) pattern, as shown in Fig. 1. SEM revealed micron-sized crystalline domains of $CH_3NH_3PbI_3$ on fused silica. Room temperature absorption revealed a band gap onset at around 770 nm and a distinct absorption peak at around 480 nm. XRD revealed 14.1° and 28.2° peaks for (110) and (220), respectively, which are characteristics for the pristine perovskite with tetragonal crystal structure at room temperature, in agreement with earlier works.[3]

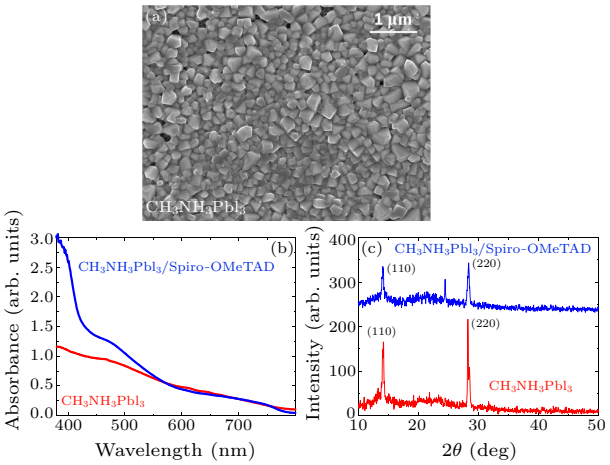


**Fig. 1.** The characterization of the thin film: (a) SEM image, (b) absorption spectra and (c) XRD pattern of the samples for THz measurements.

Our THz setup was driven by a Ti:sapphire femtosecond amplifier, operating at repetition rate of 1 kHz, and generating 120 fs pulses at central wavelength 800 nm. A portion of the laser output was split as a pump beam, after second harmonics with a $\beta$-$BaB_2O_4$ (BBO) crystal for the above band gap of the $CH_3NH_3PbI_3$ excitation at 400 nm.[24] The residual beam was used to generate and detect the THz radiation by optical rectification and electro-optical sampling using ZnTe nonlinear crystals with a frequency window of 0.3–2.0 THz. Both optical pump and terahertz probe pulses were incident on the sample at normal incidence. The in-plane conductivity of the photoexcited sample was probed with the terahertz pulse.[25–27] The terahertz spectroscopy measurement enclosure was purged with $N_2$ to minimize photo-oxidization and water vapor interference effects. No significant degradation was observed during the experiments.

The change in peak amplitude of the THz waveform is proportional to the real part of the photo-induced conductivity, mostly arising from the influence of mobile charge carriers.[28–30] By varying the time delay between the 400 nm optical pump and THz probe pulses, we acquired the dynamics of the real-valued sheet photoconductivity $\Delta\sigma_{2D}$, which can be reconstructed from the photo-induced peak change in the THz electric-field amplitude as a function of the pump-probe time delay, using a thin-film approximation known as the Tinkham equation[31]

$$\Delta\sigma_{2D} = \frac{1+n}{Z_0}\left(\frac{1}{1+\Delta E/E} - 1\right), \qquad (1)$$

where $n = 1.95$ is the THz refractive index of the fused silica substrate, and $Z_0 = 377\Omega$ is the impedance of free space.

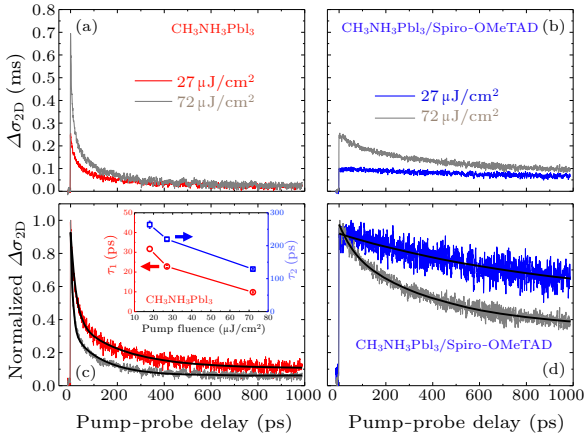


**Fig. 2.** Characteristic evolution of the pump-induced photoconductivity dynamics obtained by OPTP on (a) the $CH_3NH_3PbI_3$ neat film and (b) the $CH_3NH_3PbI_3$/Spiro-OMeTAD film. The two samples were excited at wavelength of 400 nm with fluences of 27 and 72 μJ/cm². [(c), (d)] Normalized photoconductivity transients measured at two fluences for the two samples, respectively. Thick solid lines represent bi-exponential fits of the experimental data.

Figures 2(a) and 2(b) show the photo-induced sheet real-valued conductivity $\Delta\sigma_{2D}$ of the two samples studied here for two selected pump fluences, 27 and 72 μJ/cm². The dynamics of $\Delta\sigma_{2D}$ for both the $CH_3NH_3PbI_3$ neat film and the $CH_3NH_3PbI_3$/Spiro-OMeTAD film exhibit a sharp rise immediately after the excitation within the instrumental time resolution (~120 fs). Under very similar excitation conditions, the initial value of $\Delta\sigma_{2D}$ for $CH_3NH_3PbI_3$ is around three times larger than that of $CH_3NH_3PbI_3$/Spiro-OMeTAD. As shown in Figs. 2(c) and 2(d), the maximum signal normalized to unity allows us to compare the evolution of the photoconductivity decay dynamics with exponential fits. It is important to note the difference between the two samples. For the $CH_3NH_3PbI_3$ neat film with pump fluence of

$27\,\mu J/cm^2$, the photoconductivity drops by ca. 48% within first $\tau_1 = 31.7 \pm 1.2$ ps and then 28% within $\tau_2 = 263.8 \pm 11$ ps, in contrast to a single-exponential decay of $CH_3NH_3PbI_3$/Spiro-OMeTAD film: 49% within $\tau_1 = 963 \pm 84$ ps. This observation shows that the decay pathways of the photo-induced mobile charges in the neat $CH_3NH_3PbI_3$ and that in the $CH_3NH_3PbI_3$/Spiro-OMeTAD must be different.

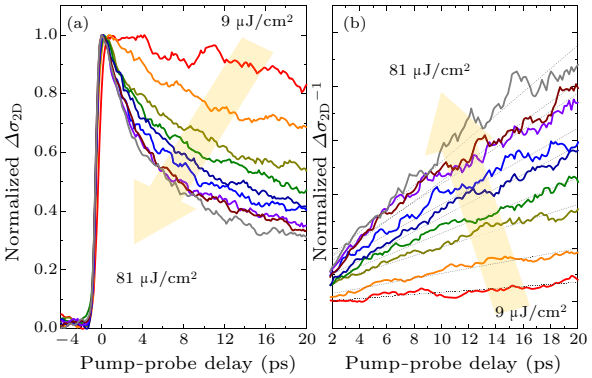


**Fig. 3.** (a) The normalized dynamical traces of neat $CH_3NH_3PbI_3$ sample at various pump fluences (9–81 $\mu J/cm^2$). (b) Reciprocal of the dynamical traces shown in (a).

We assume that the carrier mobilities do not change significantly with the pump-probe time delay, hence the decay in THz conductivity mainly reflects the temporal evolution of charge carrier density. The observed decay becomes increasingly faster as the excitation fluence increases from $9\,\mu J/cm^2$ ($N_{ph} \sim 1.57 \times 10^{17}$ photon/$m^2$) to $81\,\mu J/cm^2$ ($N_{ph} \sim 13.9 \times 10^{17}$ photon/$m^2$), as shown in Fig. 3(a). The time constants for $CH_3NH_3PbI_3$ obtained from the bi-exponential fits for pump fluences are shown in the inset of Fig. 2(c). The first-$\tau_1$ and second-exponential $\tau_2$ decay processes become faster upon increasing the pump fluence. In our experiment, the second exponential time constant $\tau_2$ decreases from 264 ps for $9\,\mu J/cm^2$ to 130 ps for $72\,\mu J/cm^2$, which can be assigned to the second-order bimolecular electron–hole recombination.[32] It is also evidenced by the linearity of $(\Delta\sigma_{2D})^{-1}$ as a function of time over the entire range of excitation fluences, as shown in Fig. 3(b). Furthermore, the first fast exponential time constant $\tau_1$ decreases with the increasing pump fluence, from 32 ps for $9\,\mu J/cm^2$ to 10 ps for $72\,\mu J/cm^2$, which can be reasonably attributed to the trimolecular Auger recombination.[32,33] On the other hand, THz conductivity transient for the $CH_3NH_3PbI_3$/Spiro-OMeTAD at low fluence ($27\,\mu J/cm^2$) is almost flat and fits well to a monoexponential ($\tau = 963 \pm 80$ ps). In this case, the second-order recombination is almost eliminated. The recombination dynamics of $CH_3NH_3PbI_3$/Spiro-OMeTAD is nearly pump fluence independent. Only at high pump fluence ($72\,\mu J/cm^2$), the data can be fitted better to a biexoponential decay with decay time constants $\tau_1 = 62 \pm 5$ ps and $\tau_2 = 426 \pm 16$ ps, which is dominantly assigned to the recombination between holes injected into Spiro-OMeTAD and mobile electrons in the perovskite.

Knowing the conductivity is defined as $\sigma = eN\mu$, where $e$ is the elementary charge, $N$ is the carrier density, and $\mu = e\tau_s/m^*$ is the mobility dependent on carrier momentum scattering time $\tau_s$ and effective mass $m^*$. In our case, therefore the product of the quantum yield $\eta$ and the sum of electron and hole mobility $\mu_{tot} = \mu_e + \mu_h$ is expressed as the effective mobility $\mu_{eff}$ by

$$\mu_{eff} = \eta \times \mu_{tot} = \frac{\Delta\sigma_{2D}}{eN_{exc}}. \quad (2)$$

Figure 4(a) shows $\Delta\sigma_{2D}$ scaled to the $e$ times excited electron density $N_{exc}$ as a function of the pump-probe delay. In the case of 400 nm optical excitation at a fluence of $27\,\mu J/cm^2$ corresponded to $N_{ph} = 4.7 \times 10^{17}$ and $4.8 \times 10^{17}$ photon/$m^2$ for $CH_3NH_3PbI_3$ and $CH_3NH_3PbI_3$/Spiro-OMeTAD, respectively. Assuming that each absorbed photon is converted into an electron–hole pair, the initial carrier density $N_{exc}$ is calculated as $N_{exc} = 2N_{ph}$.

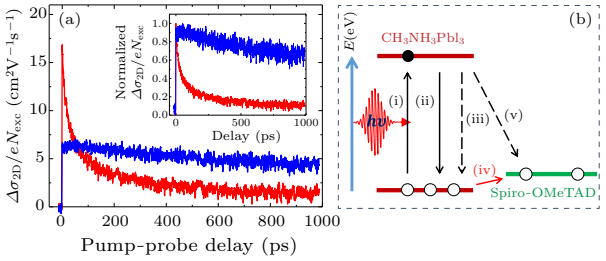


**Fig. 4.** (a) The photoconductivity signal expressed as the product of the quantum yield and the carrier mobility (inset: normalized to unity). (b) Schematic diagram of energy levels and electron relaxation and transfer processes in a perovskite/HTM sample. Electrons left in the conduction band of $MAPbI_3$ after photo-excitation (i), and then recombine with both the dark holes in the valence band of $CH_3NH_3PbI_3$, including the radiative/photoluminescence (ii) and/or the non-radiative electron-hole recombination (iii) and the photo-generated holes injected into Spiro-OMeTAD (iv) and back charge transfer at the interface between perovskite/HTM (v).

We find that the effective mobility $\mu_{eff}$ (i.e., the product of the quantum yield and total mobility) of the $CH_3NH_3PbI_3$/Spiro-OMeTAD film shows a very different photo-response dynamics at the pump fluence of $27\,\mu J/cm^2$, compared with the neat perovskite film. The peak value of $\mu_{eff}$ for the neat $CH_3NH_3PbI_3$ is 18.5 $cm^2/Vs$, very similar to that reported by Wehrenfennig *et al.*[21] and Carlito *et al.*[33] For the $CH_3NH_3PbI_3$/Spiro-OMeTAD, the initial value of $\mu_{eff}$ is about 3 times smaller (~6.5 $cm^2/Vs$) than the neat $CH_3NH_3PbI_3$ film. The reduction of the effective mobility can be well interpreted as charge transfer. In our case of $CH_3NH_3PbI_3$/Spiro-OMeTAD, where there is

ultrafast injection of holes from the perovskite into Spiro-OMeTAD, as shown in the schematic of photophysical processes in Fig. 4(b), then the total mobility will be $\mu_{\rm tot} = \mu_{\rm e,perovskite} + \mu_{\rm h,Spiro-OMeTAD}$. As previously reported, the hole mobility in Spiro-OMeTAD is $\sim 1\times10^{-4}\,{\rm cm}^2/{\rm Vs}$,[34] which is four orders smaller than that in $CH_3NH_3PbI_3$. Hence, the overall lower mobility $\mu_{\rm tot}$ obtained in the $CH_3NH_3PbI_3$/Spiro-OMeTAD is dominated by the mobility of electrons only staying in perovskite. It should be noted that the reduction in both the THz photoconductivity and the effective mobility response happens within the instrument response function, as soon as the charge carriers are photogenerated. As shown in Fig. 4(b), the offset in the valence band of Spiro-OMeTAD with respect to $CH_3NH_3PbI_3$ is around 0.21 eV, which is enough to drive this ultrafast transfer.[35] This ultrafast injection of holes also suggests the perfect electronic coupling between the Spiro-OMeTAD and the perovskite via the oxygen-containing groups.[20] Recently, such an ultrafast hole transfer was also observed in perovskite/NiO (inorganic hole extractor) interface.[16]

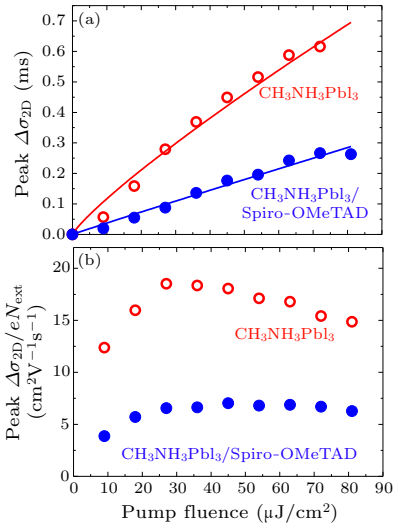


**Fig. 5.** Excitation fluence dependence of (a) $\Delta\sigma_{2D}$ and (b) $\mu_{\rm eff}$ taken at zero-delay time for neat $CH_3NH_3PbI_3$ (full circles) and $CH_3NH_3PbI_3$/Spiro-OMeTAD (open circles), respectively.

Figure 5(a) shows the peak value of real-valued photoconductivity as a function of the excitation fluence for the two samples. We observe a very weak sublinear fluence dependence of the initial photoconductivity. The best fits by a power law of the form: $\Delta\sigma_{\rm 2D,peak} = AF^B$, where $F$ is the pump fluence, and $B = 0.85 \pm 0.06$ and $0.98\pm0.08$ for neat $CH_3NH_3PbI_3$ and $CH_3NH_3PbI_3$/Spiro-OMeTAD, respectively. Compared with the conjugated polymers-based organic solar cells, of which $B \approx 0.5$, indicating that the instantaneous rise of the real conductivity at zero time can be attributed to the exciton–exciton annihilation upon photoexcitation.[36,37] In P3HT:$PC_{70}BM$, after exciton splitting, charge transfer states or polaron pairs are formed at the donor–acceptor interface on the sub-ps time scale, in which the charges still attract each other coulombically.[36] In contrast, unbound electrons and holes play a principal role in the excited-state dynamics of OMHP under photoexcitation. The efficiency of dissociation of excitons into free electrons and holes depends on the exciton binding energy ($E_{\rm b}$). The value of $E_{\rm b}$ of $CH_3NH_3PbI_3$ is rather small (estimated <10 meV), and is of the order of thermal energy at room temperature, indicating that a significant fraction of exciton will dissociate into free electron and holes right after photoexcitation. Our experimental results indicate that the rise of THz conductivity mainly comes from the free charges rather than exciton.[38–42] Figure 5(b) shows the dependence of effective mobility on the incident pump fluence. We see an initial (pump fluence $<27\,\mu{\rm J/cm}^2$) increase in the effective mobility $\mu_{\rm eff}$, up to $18.5\,{\rm cm}^2/{\rm Vs}$ and $6.5\,{\rm cm}^2/{\rm Vs}$ for the neat $CH_3NH_3PbI_3$ and $CH_3NH_3PbI_3$/Spiro-OMeTAD, respectively. As the pump fluence increases further above $27\,\mu{\rm J/cm}^2$, $\mu_{\rm eff}$ then gradually flattens off for the $CH_3NH_3PbI_3$/Spiro-OMeTAD, while it decreases on increasing pump fluence for the neat $CH_3NH_3PbI_3$, which can also be assigned to the second order recombination process.[32,33]

In addition, another important observation is shown by the normalized absolute values for the two samples in Figs. 2(c) and 2(d) and in the inset of Fig. 4(a), the rise time of the THz photoconductivity and effective mobility of $CH_3NH_3PbI_3$/Spiro-OMeTAD are very similar to those of the neat $CH_3NH_3PbI_3$ film, which suggests that the mechanism of photo-carriers generation is not altered by the presence of Spiro-OMeTAD. In contrast, $\mu_{\rm eff}$ of $CH_3NH_3PbI_3$/Spiro-OMeTAD decays much more slowly than that for neat $CH_3NH_3PbI_3$ within the first ns, indicating a different mechanism of recombination. There are several processes that could contribute to the decay path of photoexcited carriers, as shown in Fig. 4(b). For the neat $CH_3NH_3PbI_3$, the only possible pathway of photo-energy is electron–hole recombination, either through radiative or non-radiative process (processes ii and iii). Once the Spiro-OMeTAD is introduced into the $CH_3NH_3PbI_3$, hole injection (process iv) occurs as a primary charge separation step. The slow decay of $\mu_{\rm eff}$ is assigned to the back charge transfer at the $CH_3NH_3PbI_3$/Spiro-OMeTAD interface (process v).[17]

In summary, we have studied the transient THz conductivities of $CH_3NH_3PbI_3$ and $CH_3NH_3PbI_3$/Spiro-OMeTAD using time-resolved THz spectroscopy. Free charges are directly photogenerated within sub-picosecond for the two samples. Compared with $CH_3NH_3PbI_3$, the effective mobil-

ity is significantly suppressed in $CH_3NH_3PbI_3$/Spiro-OMeTAD, which demonstrates that the efficient holes transfer from perovskite into Spiro-OMeTAD on the sub-picosecond time scale, driven by the energy difference between the two materials. Rapid collection of holes by Spiro-OMeTAD helps to avoid the second-order recombination in the neat $CH_3NH_3PbI_3$ film. The slow recombination channel of $CH_3NH_3PbI_3$/Spiro-OMeTAD is dominated by the holes injected into Spiro-OMeTAD and the mobile electrons in the perovskite, named as back charge transfer at $CH_3NH_3PbI_3$/Spiro-OMeTAD interface. Our findings open the opportunity to design perovskite/HTM interfaces in devices.

## References


[1] Lee M M, Teuscher J, Miyasaka T et al 2012 *Science* **338** 643
[2] Green M A, Ho-Baillie A and Snaith H J 2014 *Nat. Photon.* **8** 506
[3] Liu M, Johnston M B and Snaith H J 2013 *Nature* **501** 395
[4] Nie W, Tsai H, Asadpour R et al 2015 *Science* **347** 522
[5] Manser J S, Christians J A and Kamat P V 2016 *Chem. Rev.* **116** 21
[6] Lin Q, Armin A, Nagiri R C R et al 2015 *Nat. Photon.* **9** 106
[7] Stranks S D, Eperon G E, Grancini G et al 2013 *Science* **342** 341
[8] Xing G, Mathews N, Sun S et al 2013 *Science* **342** 344
[9] Oga H, Saeki A, Ogomi Y et al 2014 *J. Am. Chem. Soc.* **136** 13818
[10] Yamada Y, Nakamura T, Endo M et al 2014 *J. Am. Chem. Soc.* **136** 11610
[11] Brenner T M, Egger D A and Kronik L 2016 *Int. Mater. Rev.* **1** 15007
[12] Yin W J, Shi T and Yan Y 2014 *Appl. Phys. Lett.* **104** 063903
[13] Shi D, Adinolfi V, Comin R et al 2015 *Science* **347** 519
[14] Yang Y, Yan Y, Yang M et al 2015 *Nat. Commun.* **6** 7961
[15] Wehrenfennig C, Eperon G E, Johnston M B et al 2014 *Adv. Mater.* **26** 1584
[16] Corani A, Li M H, Shen P S et al 2016 *J. Phys. Chem. Lett.* **7** 1096
[17] Marchioro A, Teuscher J, Friedrich D et al 2014 *Nat. Photon.* **8** 250
[18] Yang Y, Yang M, Li Z et al 2015 *J. Phys. Chem. Lett.* **6** 4688
[19] Manser J S and Kamat P V 2014 *Nat. Photon.* **8** 737
[20] Brauer J C, Lee Y, Nazeeruddin M K et al 2016 *J. Mater. Chem. C* **4** 5922
[21] Wehrenfennig C, Liu M, Snaith H J et al 2014 *J. Phys. Chem. Lett.* **5** 1300
[22] Deschler F, Price M, Pathak S et al 2014 *J. Phys. Chem. Lett.* **5** 1421
[23] Fang H, Wang F, Adjokatse S et al 2016 *Light: Sci. Appl.* **5** e16056
[24] Lang L, Yang J H, Liu H R et al 2014 *Phys. Lett. A* **378** 290
[25] Ulbricht R, Hendry E, Shan J et al 2011 *Rev. Mod. Phys.* **83** 543
[26] Milot R L, Eperon G E, Snaith H J et al 2015 *Adv. Funct. Mater.* **25** 6218
[27] Chan L O V, Salim T, Kadro J et al 2015 *Nat. Commun.* **6** 7903
[28] Wehrenfennig C, Liu M, Snaith H J et al 2014 *Energy Environ. Sci.* **7** 2269
[29] Valverde-Chávez D A, Jr. Ponseca C S, Stoumpos C C et al 2015 *Energy Environ. Sci.* **8** 3700
[30] Jr. Ponseca C S, Savenije T J, Abdellah M et al 2014 *J. Am. Chem. Soc.* **136** 5189
[31] Lui K P H and Hegmann F A 2001 *Appl. Phys. Lett.* **78** 3478
[32] Yettapu G R, Talukdar D, Sarkar S et al 2016 *Nano Lett.* **16** 4838
[33] Jr. Ponseca C S, Hutter E M, Piatkowski P et al 2015 *J. Am. Chem. Soc.* **137** 16043
[34] Snaith H J and Grätzel M 2007 *Adv. Mater.* **19** 3643
[35] Samrana K, Mohammad K N, Michael G et al 2014 *Angew. Chem. Int. Ed.* **53** 2812
[36] Jin Z, Gehrig D, Dyer-Smith C et al 2014 *J. Phys. Chem. Lett.* **5** 3662
[37] Dicker G, Haas M P and Siebbeles L D A 2005 *Phys. Rev. B* **71** 155204
[38] Sheng C, Zhang C, Zhai Y et al 2015 *Phys. Rev. Lett.* **114** 116601
[39] D'Innocenzo V, Grancini G, Alcocer M J et al 2014 *Nat. Commun.* **5** 3586
[40] de Quilettes D W, Vorpahl S M, Stranks S D et al 2015 *Science* **348** 683
[41] Han X W, Hou L, Yang L et al 2016 *Chin. Phys. Lett.* **33** 120701
[42] Fan Z F, Tan Z Y, Wan W J et al 2017 *Acta Phys. Sin.* **66** 087801 (in Chinese)